ISSN 0869-5938, Stratigraphy and Geological Correlation, 2015, Vol. 23, No. 5, pp. 451–467. © Pleiades Publishing, Ltd., 2015.
Original Russian Text © K.A. Savko, N.S. Bazikov, G.V. Artemenko, 2015, published in Stratigrafiya. Geologicheskaya Korrelyatsiya, 2015, Vol. 23, No. 5, pp. 3–21.

Geochemical Evolution of the Banded Iron Formations of the Voronezh Crystalline Massif in the Early Precambrian: Sources of Matter and Geochronological Constraints

K. A. Savko[a], N. S. Bazikov[a], and G. V. Artemenko[b]

[a] *Voronezh State University, Universitetskaya pl. 1, Voronezh, 394006 Russia*

[b] *Institute of Geochemistry, Mineralogy, and Ore Formation, pr. Akademika Palladina 34, Kyiv, 03680 Ukraine*

e-mail: ksavko@geol.vsu.ru

Received August 18, 2014; in final form January 19, 2015

Abstract—The banded iron formations (BIFs) of the Voronezh Crystalline Massif occur at three stratigraphic levels: Mesoarchean, Neoarchean, and Paleoproterozoic. In comparison with Paleoproterozoic BIFs, the Archean BIFs are enriched in TiO_2, Al_2O_3, Cr, Ni, and REEs. All the BIFs are characterized by positive Eu anomalies, absence of Ce anomalies, and predominance of HREEs over LREEs. The Paleoproterozoic BIFs show no evidence of clastic or hydrothermal contamination. The low Ni/Fe ratios indicate that the BIFs are younger than 2.7 Ga and their formation was followed by a sharp drop of the level of the mantle Ni supply. On the other hand, very low (<1 ppm) U contents indicate the upper age of iron accumulation—no later than the Great Oxidation Event of ~2.47 Ga.

Keywords: banded iron formations, geochemistry, trace elements, evolution, Precambrian

DOI: 10.1134/S0869593815050068

INTRODUCTION

Ferruginous quartzites, which are chemogenic sedimentary rocks, are the dominant rock type in the Precambrian BIFs. The low contents of elements accumulated in the upper and middle crust (Al, Ti, Zr, Hf, Th, U, Nb, Sc) emphasize their authigenic origin. The distribution of trace elements in BIFs is used in assessment of the composition of ancient oceans, because they precipitate along with authigenic iron hydroxides.

In spite of the long history of VCM Precambrian BIFs studying, their sedimentation age constraints are not quite certain for the purposes of geological interpretation of crustal evolution in the Early Precambrian. It is difficult to determine the age of the BIFs because of the lack of reliable geochronometers. The early attempts at using the K–Ar method to identify the age of the BIFs did not yield adequate results and most Rb–Sr ages correspond to the age of their metamorphism. The U–Pb dating of zircons from ash tuffs intercalated with BIFs and from BIF-intruded plutons is the only method of strict identification of the sedimentation age of the BIFs.

According to Golivkin et al. (*Zhelezorudnye...*, 1982), the most ancient BIFs of the VCM are of Late Archean age and correlate with Verkhovtsevo type of the BIFs of the Ukrainian Shield and with the Kola Group of the Baltic Shield. Shchegolev (1985) considered that iron rocks occur in the Early (Oboyan Group) and Late (Mikhailovskaya Group) Archean and the Early Proterozoic (Kursk Group). He ascribed the amphibole–magnetite, amphibole–garnet–magnetite, and pyroxene–magnetite BIFs in the area of Besedino, Lev-Tolstovskii, Istobnoe and some other anomalies of the magnetic field to the Archean. Kononov et al. (1988) considered that all VCM iron rocks belong to the Paleoproterozoic Kursk Group and that their different types are related to the degree of metamorphism of rocks.

It is impossible to obtain the precise isotopic ages of the BIFs of the VCM because of the absence of felsic volcanic rocks in their sections. Owing to the ambiguous position of BIFs in Early Precambrian (especially, Archean) sections and high-temperature metamorphism (amphibolite, granulite facies), there are contradictory opinions on duration of sedimentation of the BIFs of the VCM and their age (Mesoarchean, Neoarchean, or Paleoproterozoic). This problem requires solution.

Thanks to recent studies of distribution of trace and rare earth elements in the BIFs, Kohnhauser et al. (2009), Partin et al. (2013), and Bekker et al. (2014) found the age variations in their contents in Paleoarchean to Paleozoic iron rocks and showed that they depend on the dominant physicochemical conditions of the early Earth, e.g., the Great Oxidation Event (GOE) (Bekker et al., 2014) at the beginning of the Paleoproterozoic or the Snowball Earth Event in the Neoproterozoic (Kirschvink, 1992), whose age is

identified exactly. This allows us, without precision isotopic ages of the studied rocks, to determine the age of accumulation of the BIFs on the basis of new geological and geochemical data on the distribution of trace and rare earth elements in different VCM tectonic blocks.

GEOLOGICAL POSITION OF THE BANDED IRON FORMATIONS

The VCM and Ukrainian Shield form Sarmatia, which is one of three segments of the Precambrian basement of the East European craton. The VCM belongs to the northeastern part of Sarmatia and was separated from the Ukrainian Shield by the Dnieper–Donets aulacogen. Because the Ukrainian Shield and VCM were a single crust segment prior to the Paleozoic, all the extended VCM structures are traced to the Ukrainian Shield (Shchipansky and Bogdanova, 1996). The central part of Sarmatia is occupied by the Archean Sumy–Dnieper granite-greenschist domain consisting of the Middle Dnieper Block of the Ukrainian Shield and Sumy Block of the VCM (Shchipansky et al., 2007). It is rimmed by the Archean Sevsk–Kirovgrad and Oskol–Azov belts from the west and east, respectively. The Paleoproterozoic Belaya Tserkov–Odessa belt, which divides the Volyn–Podol and Kirovgrad blocks of the Ukrainian Shield, is located westward of the Sevsk–Kirovgrad belt (Shchipansky et al., 2007). The Bryansk Block of the VCM, composed of granulites and various granitic rocks, is a northern continuation of the Belaya Tserkov–Odessa belt. The granulites of the Kursk–Besedino Block of the central part of the VCM occur within the Oskol–Azov belt.

The Precambrian basement of the VCM consists of the eastern and western (Kursk) blocks, which are composed of Paleoproterozoic and Archean rocks, respectively. Paleoproterozoic rocks of the Kursk Block form the SE–NW trending narrow linear zones, which, in geodynamic respect, are interpreted as rift-related Tim-Yastrebovskaya, Mikhailovskaya, and Volotovo structures that originated on the Neoarchean protoplatform and transformed into fold synforms (Kholin, 2001).

The BIFs of the VCM are established at three stratigraphic levels: Mesoarchean, Neoarchean, and Paleoproterozoic (Shchegolev, 1985). Mesoarchean BIFs preserved between Paleoproterozoic fold synforms are established for sure only in the granulite complex of the Kursk–Besedino Block (Savko, 1999a; Fonarev et al., 2006) (Fig. 1). Neoarchean BIFs are present in the structure of the greenschist belts, which spatially coincide with Paleoproterozoic synforms, and are closely associated with amphibolites (Savko et al., 2004). Paleoproterozoic BIFs of the Kursk Group are spread the most widely at the Kursk Magnetic Anomaly (KMA) and their rocks extend as three NW-trending stripes (Tim–Yastrebovskaya, Mikhailovskaya, Volotovo) for more than 550 km (Fig. 1). All the exploited iron deposits of the KMA basin are related to the Paleoproterozoic BIFs.

The distribution of trace and rare earth elements in BIFs was studied at all stratigraphic levels, including those without clear age. The latter will be considered taking into account the conclusions based on geochemistry of these rocks. The International Chronostratigraphic Chart was used in the paper (http://www.stratigraphy.org).

Mesoarchean Banded Iron Formations

The most ancient BIFs of the VCM are present in the Kursk–Besedino Block (Shchegolev, 1985), which is located between the Paleoproterozoic extended belts (Fig. 1) and belongs to the Mesoarchean Oboyan Complex. The Kursk–Besedino Block is composed of biotite and biotite–hornblende plagiogneisses with thin interlayers of hornblende amphibolites, often migmatized. The gneiss complex is characterized by an overall mosaic pattern of its magnetic field with intense positive ellipsoid, crescent, and stripe-like magnetic anomalies (Ushakovo, Kuvshinovka, Budanovka, Besedino, and others) corresponding to various rocks which underwent metamorphism of granulite facies (Savko, 1999a, 2000; Fonarev et al., 2006): the alternating layers 1–2 to 30–35 m thick of the two-pyroxene–magnetite BIFs (locally with garnet), metapelites (spinel–garnet–cordierite–sillimanite gneisses), two-pyroxene–plagioclase, locally, garnet-bearing metagabbroic rocks, and metapyroxenites.

The concordant TIMS age of monazite from metapelite of the Kursk–Besedino Block (2819 ± 6 Ma) corresponds to the last high-temperature metamorphic event manifested in this block (Savko et al., 2010). Taking into account this circumstance, there are reasons to assume that the previous TIMS age of metamorphism of gneisses of this block (3277 ± 33 Ma, zircon monofraction; Artemenko et al., 2006) should be interpreted as an age of a detrital or early metamorphic zircon occurring in these rocks. Judging from the Sm–Nd isotopic–geochemical studies ($T_{Nd}(DM)$ = 3.24 Ga), the rocks of Paleoarchean continental crust were the source for the reviewed metapelites (Savko et al., 2010).

It should be noted that granulites of the central part of the VCM are located within the Oskol–Azov domain with tonalitic gneisses and granitic rocks with age of 3260–3360 Ma in the Azov Block and granulite metamorphism with age of 2.8–2.9 Ga (Shcherbak et al., 1995).

Neoarchean Banded Iron Formations

The data on the composition, structure, and mineralogy of the Neoarchean BIFs of VCM are limited, because it was difficult to attribute them even to the BIF–metabasite complex of the Mikhailovskaya

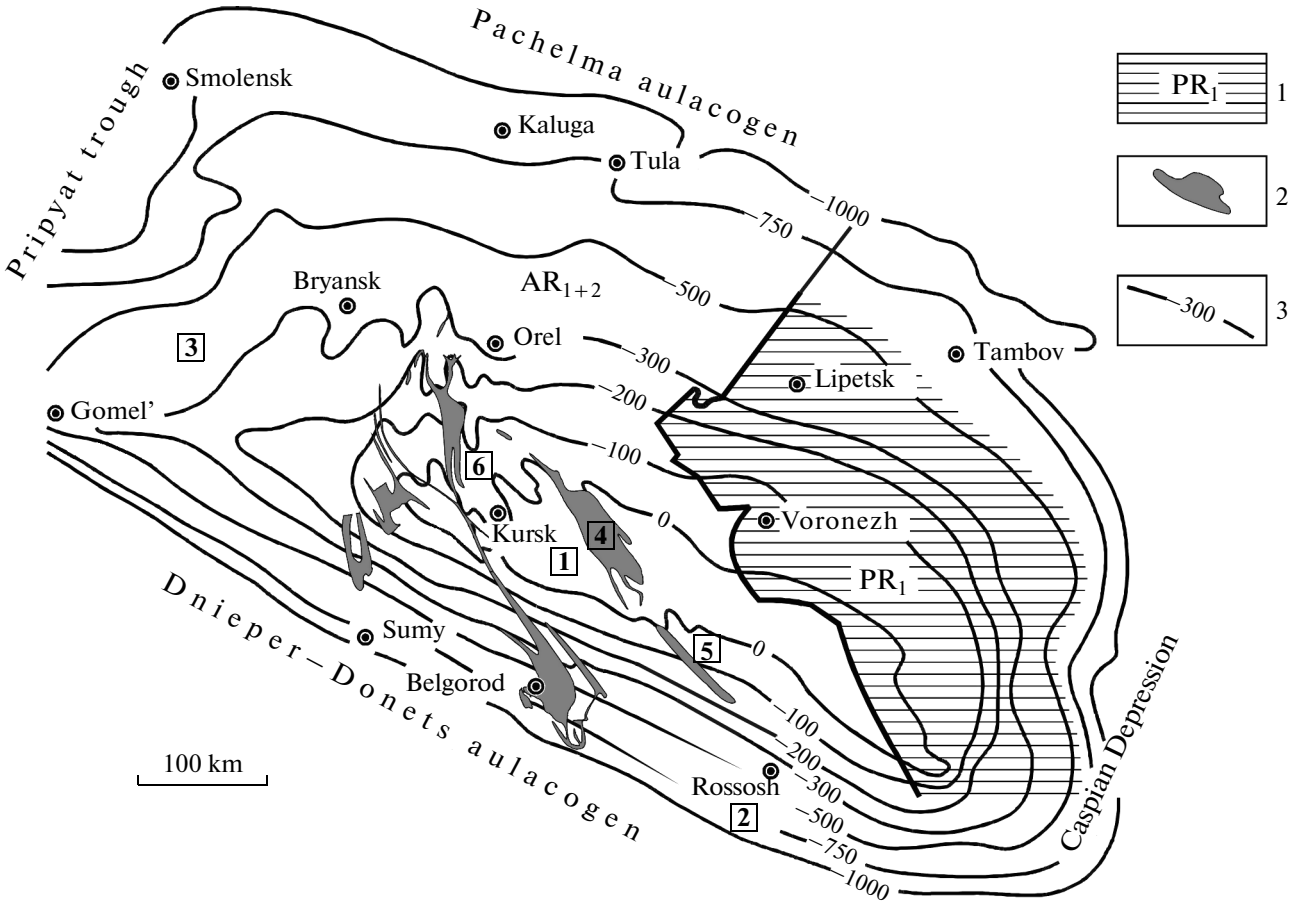

Fig. 1. Scheme of structural division of the Precambrian basement of the Voronezh Crystalline Massif, modified after (Polyakova et al., 2006). (1) Paleoproterozoic rocks of the East Voronezh province; (2) Paleoproterozoic rift structures of the Kursk Magnetic Anomaly; (3) isohypses of absolute levels of surface of the Precambrian basement. Numbers on the map: (1–3) crustal blocks: (1) Kursk–Besedino, (2) Rossosh, (3) Bryansk; (4–6) rift structures: (4) Tim–Yastrebovskaya, (5) Volotovo, (6) Mikhailovskaya.

Group (Shchegolev, 1985), since all the data on this complex were obtained during the study of drill cores of several holes and with geophysical methods.

The metamorphic mafic and rare felsic effusive rocks or gneissic sequences (e.g., Istobnoe, Medvenka, and Kodentsovo anomalies) could be the host rocks for the Neoarchean BIF complexes of the KMA. It is extremely difficult to ascribe the gneissic sequences to the Neoarchean rather than to the Mesoarchean (Oboyan Complex). It is considered that the BIFs of the Tarasovo anomalies are the most reliably belonged to the Neoarchean, because they are distinct from the Paleoproterozoic and Mesoarchean sections in a large amount of metaeffusive mafic rocks and typical structural–textural and mineralogical peculiarities of the BIFs.

The Tarasovo anomalies are located in the western part of the Kursk Block 20 km west of the Paleoproterozoic Mikhailovskaya structure (Fig. 2). They are traced for the distance of more than 20 km in a 0.5- to 3.0-km-wide anomalous strip. The beds and lenses of chlorite–amphibole(hornblende, grunerite)–magnetite BIFs are underlain and overlapped by chlorite–amphibole schists and epidote–garnet–hornblende amphibolites (metabasalts).

The BIFs occur as beds and lenses 0.5–45 m thick. The gradual transition from amphibole schists to BIFs is due to the increase in amount and thickness of quartz, amphibole, and magnetite interlayers. Interlayers of barren BIFs up to 1 m thick are locally observed at the contact with amphibole schists. The interlayers and lenses of amphibole–chlorite schists 0.5 to 10 cm (rarely up to 1 m) thick occur inside the BIFs. The banding is expressed by intercalation of amphibole–magnetite, quartz, and amphibole–quartz interlayers. Thin beds of metapelite schists and felsic metaeffusive rocks occur within the Tarasovo anomalies in addition to BIFs, amphibolites, and chlorite–amphibole schists.

The presence of clasts of volcanic rocks in the BIFs of the Tarasovo anomalies suggests their volcanic-sedimentary origin in contrast to the Paleoproterozoic chemogenic–sedimentary BIFs (Savko et al., 2004). Two metamorphic episodes are established: an early

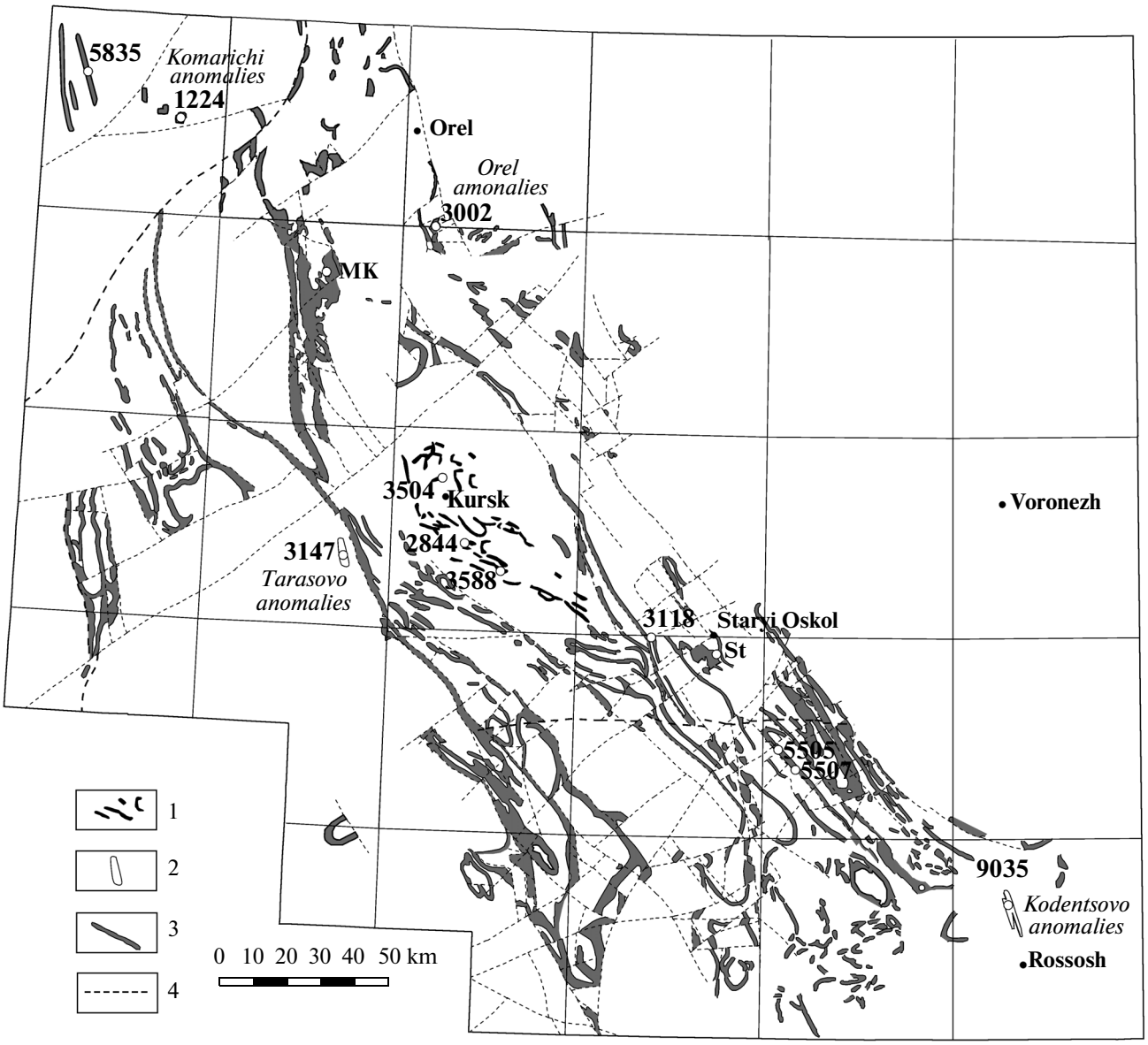

Fig. 2. Location of the Precambrian BIFs in the territory of the Voronezh Crystalline Massif. (1) Mesoarchean BIFs, (2) Neoarchean BIFs, (3) Paleoproterozoic BIFs, (4) faults. Numbers correspond to the holes from which the studied samples were taken. MK, Mikhailovskii open pit; St, Stoilenskii open pit.

high-temperature (600–650°C) and late low-temperature (450–500°C) at pressures of 4–5 kbar (Savko et al., 2004). The high-temperature episode occurred in Neoarchean or at least prior to the formation of the Paleoproterozoic BIF. The low-temperature episode was coeval with metamorphism of the Paleoproterozoic BIF within the Mikhailovskaya structure.

The Kodentsovo anomalies, which are composed of the BIFs and metapelitic gneisses of the West Kodentsovo area in the central part of the VCM probably belong to the Neoarchean Mikhailovskaya Group. The BIF sequence consists of banded hornblende–grunerite–magnetite rocks and garnet–grunerite amphibolites intercalated with biotite–garnet gneisses (Savko, 1994). The thicknesses of intercalated rocks vary from tens of centimeters to a few tens of meters. The visible thickness of the sequence of iron rocks exposed by Hole 9035 is 439 m. It is underlain by the gray hornblende plagiogneisses sharply distinct in structure and mineral and chemical composition from Ca-poor aluminous gneisses intercalated with iron rocks. Plagiogneisses presumably belong to the Oboyan Complex.

The iron rocks of the West Kodentsovo area were metamorphosed at temperature of 600–650°C and pressure of 5 kbar (Savko, 1994).

The preliminary age of zircons from gneisses in the BIF structure (Holes 9035 and 9038) is no less

than 2.7 Ga (our unpublished data). The Kodentsovo BIFs described are located in the Kodentsovo–Pokrovskii greenschist belt; on one hand, they differ in structure of sections from the Paleoproterozoic BIFs, and, on the other hand, it is impossible to ascribe them to the Mesoarchean by the age of zircons. Thus, we attribute them presumably to the Neoarchean.

Paleoproterozoic Banded Iron Formations

Paleoproterozoic BIF sections are the most well studied in the Tim–Yastrebovskaya, Mikhailovskaya, and Volotovo structures with numerous research and exploration holes and open pits of the exploited deposits. The Paleoproterozoic BIF of the Kursk Group consists exclusively of chemogenic-sedimentary (Fe–Si) and terrigenous-sedimentary rocks, which compose the wings of the large Paleoproterozoic Tim–Yastrebovskaya, Mikhailovskaya, and Volotovo structures. The Kursk Group is composed of the Lower Stoilenskaya and Upper Korobkovskaya formations. The Stoilenskaya Formation occurs with clear unconformity on the Archean gneisses or Neoarchean K-rhyolites in the basement of the Paleoproterozoic section of the Kursk Block. The terrigenous-sedimentary rocks of the Stoilenskaya Formation underlie the Fe-bearing sequence of the Korobkovskaya Formation and consist of two subformations. The lower subformation consists of gray and light gray fine-grained quartz metasandstones with lenses and interlayers of quartz metaconglomerates and metagravelites in the basement. The upper subformation is composed of carbonaceous shales with interlayers of metasandstones. The thickness of the formation varies from several meters in the antiform structures to hundreds of meters in large synforms.

The Korobkovskaya iron formation with thickness from a few meters to 1200 m and more conformably occurs on the Stoilenskaya Formation and with erosion is overlapped by rocks of the Oskol Group. In the most complete sections, the Korobkovskaya Formation consists of alternated sequences of BIFs and shales with a total thickness of more than 1 km. In spite of lateral variability in the BIF sections, we accept its four-membered structure: the first and third subformations are iron members, which are divided and overlapped by the shale (second and fourth) subformations.

The lower (first) BIF subformation up to 750 m thick is mostly composed of magnetite, grunerite–magnetite, riebeckite–magnetite, and carbonate–magnetite rocks. The interlayers of almost barren and barren rocks up to 5–10 m thick occur at the bottom, at the top, and inside of the subformation near the shale interlayers.

The lower (second) subformation of shales 0–10 to 120 m thick (rarely more) divides the BIF subformations and is composed of carbonaceous–quartz–micaceous (often with phyllite), quartz–biotite, and quartz–muscovite shales with pyrite and pyrrhotite, locally, with garnet and andalusite.

The upper (third) BIF subformation with thickness from a few tens of meters to 500–870 m is mostly composed of hematite–magnetite rock with subordinate magnetite–hematite, hematite, grunerite–magnetite, riebeckite–magnetite, and carbonate–magnetite interlayers.

The upper (fourth) subformation crowns the section of the Kursk Group. It occurs only in large synforms and is partly preserved from erosion at the Novoyaltinskoe, Mikhalovskoe, Lebedinskoe, and Stoilenskoe deposits. The subformation 0–400 m thick consists of carbonaceous–micaceous, quartz–muscovite, quartz–chlorite–muscovite, and quartz–muscovite–carbonate shales.

Paleoproterozoic BIFs are distinct from Archean ones in more diverse mineralogical composition. Rocks with tetraferribiotite, stilpnomelane, seladonite, ferrishamosite, riebeckite, grunerite, ferriwinchite, actinolite, aegirine, Na-diopside, and carbonates (calcite, ankerite–dolomite series, siderite) are abundant in addition to hematite, hematite–magnetite, and magnetite BIFs (Savko and Poskryakova, 2003; Savko, 2006). Orthopyroxene may appear in zones of higher metamorphism. The Al-bearing minerals (garnets, plagioclases, hornblendes, chlorites), excluding biotite, are absent in the Paleoproterozoic BIF of the VCM.

The precise age of iron sedimentation of the Kursk Group is unknown. The conglomerates of the Stoilenskaya Formation occur on the weathered quartz porphyry rocks with age of 2612 ± 10 Ma (SIMS; zircon; Savko et al., 2015). The upper boundary of accumulation of Fe-bearing sequences may be determined by the age of overlapping metarhyolites of the Kurbakinskaya Formation of the Oskol Group in the Mikhailovskaya structure (2050 Ma, TIMS, zircons; Artemenko, 1998) or by the age of granodiorites of the Stoilo-Nikolaevskii Complex in the Tim–Yastrebovskaya structure (2.04–2.05 Ga; SIMS; zircons; Savko et al., 2014) intruding the rocks of the Kursk and Oskol groups.

The age of highly metamorphosed BIFs of the Bryansk Block was considered to be Archean for a long time; however, it was found that the U–Pb age of the detrital zircons from metapelites intercalated with BIF is 2560 Ma (TIMS, monofractions). The Sm–Nd model age (bulk sample) of the protolith of granulites of the Bryansk Block is 2630 Ma and the age of their metamorphism is 2.1–2.3 Ga (Bibikova et al., 1995). These ages are the lower limits of accumulation of sedimentary sequences of the terrane. The age of granulitic metamorphism of 2036 ± 4 Ma (TIMS; monazites; Savko et al., 2010) could be the upper limit. The results of our Sm–Nd isotopic–geochemical studies show that the protoliths of granulites of this block were formed as a result of reworking of rocks of the continental crust with the average Sm–Nd model age of

3.4 Ga (Savko et al., 2010). This allows us to consider the Bryansk Block as part of a Paleoproterozoic structure that originated on the Paleo- and Mesoarchean continental crust of the ancient core of Sarmatia.

Aluminous graphite gneisses, calcareous–silicate rocks, phlogopite–diopside marbles, and orthopyroxene plagiogneisses metamorphosed at temperature of 850°C and pressure of 6 kbar occur in the BIF sections (Hole 5835) in addition to pyroxene–magnetite rocks (Savko and Lebedev, 1996; Savko, 1999b). Thus, the BIFs of the Bryansk Block are similar in variety of rocks to highly metamorphosed Paleoproterozoic BIFs and are distinct from Archean BIFs (Kursk–Besedino Block, Tarasovo anomalies); hence, we consider them as Paleoproterozoic, which underwent intense high-temperature reworking.

The hyperstene–magnetite BIFs of the Komarichi magnetic anomalies located in the southeastern continuation of the Bryansk Block were previously ascribed to the Archean because of the high metamorphism. Taking into account the aforementioned data, we believe that these BIFs are Paleoproterozoic.

METHODS OF STUDY

Because the BIF rocks of the VCM are not exposed, all the samples from the Mesoarchean and Neoarchean and the greater part of the Paleoproterozoic BIFs came from drill cores. Samples MK-2, MK-9, 466-p/224, ST-1, and ST-2 were collected from the open pits of the Mikhailovskoe and Stoilenskoe iron deposits, respectively.

The chemical composition of the samples was analyzed on a PW-2400 sequential spectrometer (Philips Analytical B.V.) at the Institute of Geology of Ore Deposits, Petrography, Mineralogy, and Geochemistry, Russian Academy of Sciences (Moscow). The spectrometer was calibrated using branch and state standard samples of chemical composition of rocks and mineral raw materials (14 OSO, 56 GSO). The samples for analysis of major oxides were prepared by melting of 0.3 g of powder of the sample with 3 g Li tetraborate in an inductive oven with further production of a homogenous glassy disk. The accuracy of analysis was 1–5 and up to 12 rel. % for elements with contents higher and lower than 0.5 wt %, respectively.

The trace elements were analyzed by ICP-MS at the Analytical Certified Experimental Center of the Institute of Microelectronic Technology and High Purity Materials, Russian Academy of Sciences (Chernogolovka). The samples of rocks depending on their composition were decomposed by acid opening in both open and closed systems. The detection limits were 0.02–0.03 ppm for REEs, Hf, Ta, Th, and U; 0.03–0.05 ppm for Nb, Be, and Co; 0.1 ppm for Li, Ni, Ga, and Y; 0.2 ppm for Zr; 0.3 ppm for Rb, Sr, and Ba; and 1–2 ppm for Cu, Zn, V, and Cr. The analyses were controlled by measurements of international and Russian GSP-2, BM, SGD-1A, and ST-1 standards. The errors of analyses were 3 to 5 wt % for most elements.

GEOCHEMISTRY OF THE BANDED IRON FORMATIONS OF THE VCM

The mineral composition of samples analyzed is given in Table 1.

The Mesoarchean BIFs. Two-pyroxene–magnetite rocks, locally with grunerite and garnet, metamorphosed under conditions of high-temperature granulite facies were sampled in the Kursk–Besedino Block. These are dense, medium- to coarse-grained, gray and greenish gray rocks with massive, banded, and vague-banded structures and granoblastic, locally, with elements of porphyroblastic texture. The banded structures are caused by oriented arrangement of minerals as alternating, often broken bands with thickness from a few millimeters to 3–4 cm.

The rocks are characterized by a high content of Fe_2O_{3total} (45–61 wt %) and SiO_2 (32–50 wt %). The contents of other major oxides are less than 3.5 wt % (Table 2). We also analyzed pyroxene BIFs of the West Azov region, because they are located in the same tectonic zone with the BIFs of the Kursk–Besedino Block and are characterized by similar chemical composition (Table 2).

The Mesoarchean BIFs exhibit widely variable low contents of REEs (7–60 ppm, 35 ppm on average), positive Eu/Eu* and Y_{SN} anomalies, enrichment in HREEs relative to LREEs $(Pr/Yb)_{SN}$ = 0.31–1.02, 0.56 on average) (Table 3, Fig. 3), high Y/Ho ratios (27–58, 33 on average) exceeding the chondrite ratio (~28) (Table 3), and absence of clear Ce anomalies (Ce/Ce*). The Ni/Fe molar ratios are high (0.21–0.68×10^{-4}, up to 5.71×10^{-4} in several samples with terrigenous material). Many samples have low contents of Al_2O_3 (<1 wt %), TiO_2 (0.01–0.20 wt %, 0.06 wt % on average), Cr (4–46 ppm), Zr (5–16 ppm), and V (6–17 ppm) indicating a minimal supply of terrigenous material in primary chemogenic sediments. Three samples of rocks with garnet (Table 1; Samples 2844/192, 288/194, 3588/213.5) and higher contents of Al_2O_3 (1.1–3.5 wt %) (Table 2), however, are enriched in TiO_2 (0.21–0.29 wt %), Cr (102–228 ppm), Zr (14–97 ppm), V (38–109 ppm), and Co (12–24 ppm) (Table 3, Fig. 4), which suggests insignificant presence of clastic material.

The Neoarchean BIFs. In the volcanic sequence of the Tarasovo anomalies, they include amphibole (hornblende, grunerite)–magnetite rocks with higher contents of SiO_2 (49–64 wt %), Al_2O_3 (2.8–6.0 wt %), and MgO (1.8–4.6 wt %) and lower contents of Fe_2O_{3total} (29–38 wt %) in comparison with Mesoarchean BIFs (Table 2). The TiO_2 contents are similar to those of Mesoarchean BIFs with terrigenous material.

The Neoarchean rocks show higher contents of REEs (45–74 ppm, 55 ppm on average), significant positive Eu anomalies (Eu/Eu* = 1.34–1.61; Table 3, Fig. 3),

Table 1. Mineral composition of BIFs

Sample number	Qtz	Mag	Hem	Opx (Cpx)	Gru	Grt	Bt	Ab	Hbl	Act	Sld	Chl	Cal	Fe-Dol	Aeg	Rbk
	Kursk–Besedino Block															
3504/260.2	+	+		+												
3588/221.5	+	+		+	+											
3588/213.5	+	+		+	+	+	+									
3588/230.5	+	+		+	+											
2844/192	+	+			+	+										
2844/194	+	+		+	+	+										
2844/203	+	+		+	+		+									
	West Azov region															
7/67	+	+		+	+			+								
10/307	+	+		+	+											
91/254	+	+		+	+											
10/397	+	+		+	+			+								
	Tarasovo anomalies															
3147/408	+	+			+		+		+			+				
3147/430.5	+	+			+		+		+			+				
3147/436	+	+			+		+		+			+				
	Kodentsovo anomalies															
9035/302	+	+			+		+		+							
	Komarichi anomalies															
1224/226	+	+		+												
1224/229	+	+		+												
	Orel amonalies															
3002/416	+	+	+											+		
	Volotovo structure															
5507/18	+	+	+										+		+	+
5505/35	+	+	+							+			+		+	+
	Tim–Yastrebovskaya structure															
St-1	+	+	+												+	+
St-2	+	+	+												+	+
3118/292	+	+														
3118/538	+	+														
	Mikhailovskaya structure															
MK-2	+	+	+								+		+			+
MK-9	+	+	+													
	Bryansk Block															
5835/583.5	+	+			+											

Symbols of minerals: Qtz, quartz; Mag, magnetite; Hem, hematite; Opx, orthopyroxene; Cpx, clinopyroxene; Gru, grunerite; Grt, garnet; Bt, biotite; Ab, albite; Hbl, hornblende; Act, actinolite; Sld, seladonite; Chl, chlorite; Cal, calcite; Fe-Dol, Fe-dolomite; Aeg, aegirine; Rbk, riebeckite.

Table 2. Contents of major oxides (wt %) in the Precambrian BIFs of the Kursk Magnetic Anomaly and West Azov region of the Ukrainian Shield

Age	AR_1									
Object	Kursk–Besedino Block						West Azov region			
Components \ Sample number	3504/260.2	3588/221.5	3588/230.5	2844/194	2844/203	3588/213.5	1/7/67	2/10/307	3/91/254	5/10/397
SiO_2	32.17	48.82	41.56	49.99	45.22	45.64	48.92	46.48	40.50	46.07
TiO_2	0.20	0.02	0.01	0.29	0.05	0.21	0.13	0.01	0.08	0.03
Al_2O_3	0.87	0.65	0.43	3.50	1.07	1.31	0.84	0.46	0.48	0.61
Fe_2O_3	60.75	44.75	53.02	39.16	48.66	44.88	22.5	28.48	32.4	18.95
FeO	–	–	–	–	–	–	19.60	17.45	19.40	25.98
MgO	2.13	3.11	3.37	1.92	1.48	2.40	2.39	1.77	2.95	3.23
MnO	0.176	0.224	0.290	0.590	0.336	0.876	0.27	0.21	0.4	0.31
CaO	3.48	1.81	0.99	3.04	1.96	2.55	2.94	1.81	2.5	2.82
Na_2O	–	–	–	0.10	0.05	0.06	0.1	0.19	0.25	0.10
K_2O	–	–	–	0.07	0.02	0.04	0.1	0.1	0.16	0.05
P_2O_5	0.18	0.38	0.14	0.06	0.04	0.17	0.28	0.19	0.14	0.64
LOI	n.a.	n.a.	n.a.	1.12	1.05	1.37	1.26	2.44	0.37	0.67
Total	99.96	99.76	99.81	99.84	99.94	99.51	99.33	99.59	99.63	99.51

Age	AR_2				PR_1							
Object	Tarasovo anomalies				Komarichi anomalies		Orel amonalies	Mikhailovskaya structure			Tim–Yastrebovskaya structure	
Components \ Sample number	3147/408	3147/430.5	3147/436	3147/404	1224/226	1224/229	3002/416	MK-2	MK-9	466-p/244	3118/292	3118/538
SiO_2	52.3	49.16	51.74	63.85	32.83	38.03	43.78	47.46	52.14	52.06	44.12	49.07
TiO_2	0.14	0.19	0.19	0.11	0.02	–	0.04	0.01	0.01	0.02	0.02	0.01
Al_2O_3	3.76	5.91	6.02	2.79	0.38	0.32	0.88	0.18	0.27	0.43	0.22	0.27
Fe_2O_3	38.35	37.14	34.65	29.35	59.88	57.65	49.86	51.31	48.57	43.86	56.45	48.84
FeO	–	–	–	–	–	–	–	–	–	–	–	–
MgO	3.76	4.38	4.64	1.80	0.23	0.28	1.68	1.46	0.15	0.93	0.49	1.2
MnO	0.164	0.166	0.157	0.097	0.073	0.058	0.157	0.03	0.02	0.04	0.02	0.06
CaO	0.97	1.43	1.66	0.47	3.07	1.53	2.91	1.05	0.25	1.50	0.13	2.47
Na_2O	0.06	0.26	0.37	0.04	–	–	0.06	0.47	0.08	0.43	0.1	0.12
K_2O	0.12	0.23	0.38	0.07	0.02	0.04	0.10	0.19	0.14	0.04	0.03	0.05
P_2O_5	0.06	0.12	0.06	0.11	0.04	0.04	0.25	0.47	0.08	–	0.1	0.12
LOI	n.a.	n.a.	n.a.	n.a.	3.44	2.02	0.26	n.a.	n.a.	0.66	n.a.	n.a.
Total	99.68	98.99	99.87	98.69	99.98	99.97	99.98	102.63	101.71	99.97	101.68	102.21

Table 3. Contents of trace elements (ppm) in the Precambrian BIFs of the Kursk Magnetic Anomaly and West Azov region of the Ukrainian Shield

Age	AR_1										
Object	Kursk–Besedino Block							West Azov region			
Sample number / Components	3504/ 260.2	3588/ 221.5	3588/ 230.5	2844/ 192	2844/ 194	2844/ 203	3588/ 213.5	1/7/ 67	2/10/ 307	3/91/ 254	5/10/ 397
Li	2.9	0.61	0.44	1.6	1.9	1.9	0.92	2.2	7.2	2.4	n.a.
Be	0.60	0.59	0.54	0.18	0.51	0.26	1.9	0.45	0.9	0.46	0.53
Sc	1.7	0.40	0.50	9.6	8.9	1.5	4.2	1.2	1.3	0.6	Í.î.
V	7.1	8.5	6.4	109	63.1	8.8	37.6	16.7	12.8	9.3	12.9
Cr	7.6	5.4	13.0	218	228	45.6	102	3.9	8.9	21.9	22.7
Co	2.1	8.9	7.2	23.9	12.4	3.4	12.8	5.9	2.8	2.5	3.32
Ni	9.4	19.6	11.6	145	73.7	20.3	63.7	16.7	14.6	27.2	13.8
Cu	14.9	27.7	18.9	58.2	12.1	9.4	45.9	9.1	23.2	15.6	6.95
Zn	83.5	96.8	157	100	51.5	36.1	78.8	112	56.5	20.4	17.5
Ga	6.5	1.9	1.5	11.6	8.5	2.3	3.3	7.6	1.2	0.92	1.91
As	0.11	0.66	0.53	0.41	0.29	0.53	3.7	<d.l.	2.2	13	Í.î.
Rb	0.47	0.55	2.4	1.3	1.8	1.0	0.74	1.5	3.9	0.5	0.52
Sr	16.0	13.3	11.1	9.8	11.3	18.0	7.3	9	35.3	38.2	24.8
Y	11.0	10.8	8.6	10.2	9.3	4.7	7.6	14.8	10.4	3.9	8.41
Zr	5.4	15.8	10.8	97.3	13.6	6.0	25.8	14.6	4.9	6.9	2.58
Nb	3.8	1.1	0.65	5.6	2.4	0.79	0.3	3.5	0.4	0.65	2.36
Mo	2.9	2.2	1.6	1.8	1.3	0.40	1.2	3.5	1.1	1.3	1.26
Cs	0.022	0.033	0.061	0.033	0.0	0.0	0.0	0.065	0.87	0.1	n.a.
Ba	11.5	6.7	11.5	141	49.8	12.5	7.9	83.2	53.2	7	9.77
La	7.9	11.5	4.7	6.8	5.6	1.5	7.7	6.4	5.4	1.3	3.38
Ce	20.7	24.4	10.6	14.7	11.9	3.3	14.9	17.4	9.8	2.7	8.03
Pr	2.7	2.8	1.2	1.9	1.4	0.39	1.6	2.3	1.2	0.23	1.03
Nd	11.3	11.3	5.1	8.7	5.8	1.7	6.7	9.8	5.2	1.2	4.79
Sm	2.5	2.2	1.1	2.4	1.3	0.36	1.4	2.3	1.2	0.22	1.19
Eu	0.26	0.78	0.32	0.43	0.38	0.13	0.41	0.58	0.5	0.14	0.60
Gd	2.2	2.4	1.4	2.8	1.4	0.45	1.40	2.6	1.6	0.3	1.46
Tb	0.33	0.32	0.20	0.38	0.21	0.071	0.20	0.42	0.26	0.042	0.24
Dy	2.0	1.8	1.3	2.0	1.3	0.46	1.1	2.6	1.6	0.28	1.68
Ho	0.38	0.39	0.29	0.38	0.28	0.10	0.24	0.56	0.38	0.068	0.35
Er	1.04	1.09	0.90	1.02	0.88	0.38	0.69	1.8	1.2	0.24	1.10
Tm	0.14	0.14	0.13	0.14	0.12	0.054	0.10	0.27	0.17	0.034	0.16
Yb	0.89	0.87	0.88	0.94	0.85	0.37	0.63	1.93	1.2	0.22	1.07
Lu	0.15	0.12	0.14	0.14	0.13	0.06	0.10	0.26	0.17	0.038	0.16
Hf	0.22	0.30	0.14	2.69	0.44	0.16	0.69	0.24	0.09	0.089	0.07
Ta	0.25	0.056	0.020	0.34	0.17	0.065	0.039	0.15	<d.l.	0.027	n.a.
W	0.59	0.75	36.1	0.46	0.33	0.27	0.69	0.32	0.79	1	0.27
Pb	1.9	1.7	4.1	3.62	0.90	0.67	7.3	0.62	3.3	1	0.63
Bi	<d.l.	0.044	0.17	<d.l.	<d.l.	0.006	0.045	0.028	0.037	0.013	Í.î.
Th	0.29	0.40	1.4	2.6	0.36	0.10	1.4	0.68	0.52	0.2	0.27
U	0.13	0.21	1.0	0.2	0.045	0.029	0.40	0.6	1.3	0.1	0.18
Eu/Eu*	0.52	1.59	1.24	0.78	1.32	1.56	1.39	1.12	1.70	2.57	2.14
^{1}Ce/Ce*	1.01	1.00	1.04	0.94	0.98	0.98	0.98	1.02	0.89	1.13	0.98
ΣREE	52.39	60.15	28.21	42.75	31.55	9.31	37.06	49.22	29.88	7.01	25.20
Y/Ho	28.57	27.86	29.47	26.53	33.66	44.41	31.35	26.43	27.37	57.35	24.03
$(LREE/HREE)_n$	0.87	1.15	0.63	0.85	0.73	0.55	1.01	0.58	0.58	0.70	0.60
Molar $(Ni/Fe) \times 10^{-4}$	0.21	0.59	0.30	5.71	2.55	0.56	1.93	0.51	0.41	0.68	0.39
$(Pr/Yb)_{SN}$	0.97	1.02	0.46	0.64	0.53	0.34	0.81	0.38	0.32	0.33	0.31
$(Sm/Yb)_{SN}$	1.40	1.30	0.63	1.31	0.78	0.49	1.11	0.61	0.51	0.51	0.57

Table 3. (Contd.)

Age	AR_2					PR_1		
Object	Tarasovo anomalies			Kodentsovo anomalies		Komarichi anomalies		Orel amonalies
Components \ Sample number	3147/408	3147/430.5	3147/436	9035/302	9035/554	1224/226	1224/229	3002/416
Li	2.6	4.2	4.9	19.8	24.7	10.5	14.5	1.8
Be	1.1	1.4	3.1	0.50	0.30	0.17	0.33	0.83
Sc	7.1	5.9	7.3	4.3	2.9	<d.l.	<d.l.	0.6
V	51.4	56.7	39.1	11.8	25.1	1.3	<d.l.	7.5
Cr	31.7	48.8	46.5	37.2	52.9	3.5	2.1	9.1
Co	9.2	13.5	10.9	4.8	10.0	1.6	0.79	0.7
Ni	41	75.4	53.3	20.1	33.0	3.9	3.4	4.4
Cu	28.1	184		20.7	49.3	3.5	7.7	6.4
Zn	184	149	157	67.0	34.9	32.4	42.3	31.2
Ga	5.9	8	6.9	8.7	9.5	0.51	0.72	1.7
As	2.6	4.2	4.9	0.47	0.57	0.21	0.53	1.8
Rb	10.8	7.5	13.4	43.5	59.5	0.5	1.3	10.0
Sr	105	13.9	11.3	91.4	52.9	60.5	32.3	17.6
Y	9.2	16	9.1	13.5	5.1	5.4	3.7	7.8
Zr	16.6	40.5	33.4	60.1	308	2.5	2.0	11.7
Nb	1.5	2.1	2.2	2.3	4.7	0.21	1.4	0.84
Mo	0.32	0.73	0.57	1.3	1.5	0.54	1.2	0.41
Cs	0.57	1.9	3	3.5	1.5	0.019	0.028	2.9
Ba	65.2	49.6	81.2	504	501	9.8	33.3	10.6
La	13.6	8.4	9.3	17.4	29.3	4.4	1.8	3.6
Ce	37.5	17.7	18.9	32.5	55.2	7.3	3.0	7.5
Pr	3	1.9	2.1	3.7	5.2	0.81	0.35	0.86
Nd	11.4	7.6	8.1	13.1	20.3	3.3	1.6	3.7
Sm	2	1.5	1.5	2.5	3.2	0.58	0.30	0.84
Eu	0.57	0.48	0.53	0.39	0.39	0.42	0.24	0.36
Gd	2	1.9	1.6	2.0	2.3	0.74	0.43	1.0
Tb	0.3	0.32	0.24	0.36	0.30	0.10	0.059	0.16
Dy	1.6	2.1	1.4	2.2	1.2	0.57	0.41	1.1
Ho	0.3	0.46	0.3	0.50	0.18	0.12	0.090	0.24
Er	0.84	1.4	0.88	1.6	0.51	0.36	0.27	0.82
Tm	0.11	0.19	0.12	0.26	0.075	0.040	0.034	0.12
Yb	0.73	1.2	0.84	1.7	0.52	0.21	0.23	0.76
Lu	0.11	0.18	0.12	0.28	0.091	0.026	0.035	0.12
Hf	0.49	1.2	1	1.9	7.9	0.043	0.042	0.30
Ta	0.09	0.17	0.14	0.19	0.38	0.085	0.19	0.069
W	0.94	0.47	0.4	0.64	1.0	0.84	0.40	0.32
Pb	4.9	2.8	2.6	8.1	15.0	5.5	4.5	2.6
Bi	0.03	0.04	0.01	0.14	0.064	0.013	<ÏÎ	0.031
Th	1.7	2.7	2.2	5.6	10.1	0.07	0.12	1.0
U	0.81	0.75	0.59	0.81	2.8	0.73	0.14	0.20
Eu/Eu*	1.34	1.34	1.61	0.81	0.68	3.00	3.14	1.80
Ce/Ce*	1.35	1.02	0.99	0.94	1.02	0.88	0.87	0.97
ΣREE	74.06	45.33	45.93	78.48	118.75	18.98	8.71	21.14
Y/Ho	30.67	34.78	30.33	26.88	27.82	44.86	41.59	32.40
$(LREE/HREE)_n$	1.34	0.64	0.99	0.75	2.55	1.43	0.90	0.61
Molar $(Ni/Fe) \times 10^{-4}$	1.45	2.75	2.09	0.54	–	0.09	0.08	0.12
$(Pr/Yb)_{SN}$	1.31	0.51	0.80	0.69	3.17	1.22	0.49	0.36
$(Sm/Yb)_{SN}$	1.39	0.64	0.91	0.74	3.10	1.39	0.66	0.56

Table 3. (Contd.)

Age	PR_1									
Object	Volotovo structure		Mikhailovskaya structure			Tim–Yastrebovskaya structure				Bryansk Block
Sample number / Components	5507/18	5505/35	MK-2	MK-9	466-p/244	St1	St2	3118/292	3118/538	5835/583.5
Li	17.4	75.8	1.3	<d.l.	4.6	40.5	24.7	2.1	2.5	1.0
Be	0.37	0.62	0.69	0.53	0.62	4.4	2.3	0.63	0.48	0.91
Sc	1.0	<d.l.	<d.l.	<d.l.	<d.l.	1.6	<d.l.	<d.l.	<d.l.	0.67
V	15	11.2	22.7	53.3	16.7	102.9	10.6	20.7	22.1	<d.l.
Cr	22.9	6.9	34.2	27.0	17.3	16.6	8.4	15.3	18.0	12.6
Co	1.3	1.3	26.1	6.0	0.77	2.0	0.42	2.5	3.2	1.6
Ni	13.8	8.9	<d.l.	<d.l.	1.1	17.2	2.8	3.2	<d.l.	11.1
Cu	7.1	4.9	25.8	10.6	<d.l.	7.2	9.2	3.5	3.5	10.4
Zn	60.9	61.6	5.6	4.9	4.4	72.1	32.2	6.9	10.4	65.1
Ga	1.8	2.1	0.36	0.46	0.9	3.2	1.5	0.56	0.43	2.3
As	<d.l.	2.2	0.38	1.4	0.1	1.0	0.93	1.5	<d.l.	1.1
Rb	12.2	1.6	8.5	1.8	2.6	3.4	1.3	0.5	2.1	0.68
Sr	34.7	38.0	23.9	10.2	22.3	58.5	22.6	2.3	10.7	11.0
Y	4.8	4.8	0.88	1.04	0.65	14.7	5.2	2.27	1.53	6.5
Zr	26.2	7.6	1.1	1.5	3.5	97.0	24.5	2.3	1.5	7.4
Nb	1.4	2.5	0.18	0.18	0.30	115	10.4	0.20	0.12	0.71
Mo	0.50	0.57	<d.l.	1.33	0.10	0.27	0.29	<d.l.	<d.l.	0.54
Cs	2.1	0.59	0.16	0.065	0.46	0.40	0.11	0.10	0.53	<d.l.
Ba	36.5	7.8	147	17.0	11.4	173	40.0	6.0	7.0	11.0
La	3.3	1.7	1.7	2.4	1.1	1.2	1.1	1.6	1.7	3.7
Ce	6.7	3.9	2.6	3.7	2.0	2.8	2.5	2.3	2.5	6.7
Pr	0.8	0.5	0.28	0.40	0.21	0.3	0.3	0.24	0.25	0.77
Nd	3.6	1.9	1.0	1.4	0.50	1.3	1.2	0.8	0.8	3.0
Sm	0.75	0.45	0.20	0.22	0.09	0.43	0.30	0.17	0.16	0.62
Eu	0.22	0.16	0.19	0.16	0.04	0.21	0.10	0.09	0.09	0.45
Gd	0.79	0.55	0.18	0.17	0.06	1.6	0.4	0.22	0.20	0.81
Tb	0.12	0.087	0.023	0.023	0.013	0.43	0.11	0.037	0.065	0.12
Dy	0.65	0.59	0.11	0.12	0.046	3.5	0.81	0.24	0.16	0.89
Ho	0.17	0.15	0.030	0.035	0.016	0.67	0.24	0.069	0.044	0.20
Er	0.57	0.48	0.10	0.12	0.063	1.8	0.80	0.27	0.15	0.63
Tm	0.092	0.071	0.016	0.018	0.011	0.31	0.13	0.037	0.021	0.089
Yb	0.70	0.60	0.091	0.11	0.05	2.2	0.76	0.26	0.11	0.58
Lu	0.11	0.089	0.018	0.020	<d.l.	0.33	0.14	0.045	0.020	0.090
Hf	0.31	<d.l.	<d.l.	<d.l.	0.05	2.32	0.27	<d.l.	<d.l.	0.12
Ta	<d.l.	<d.l.	<d.l.	<d.l.	<d.l.	<d.l.	<d.l.	<d.l.	<d.l.	0.067
W	0.27	0.43	0.65	1.6	0.1	5.4	1.0	0.57	2.1	0.80
Pb	4.9	4.4	0.091	1.0	0.8	6.5	2.0	1.0	0.72	0.50
Bi	0.053	0.050	<d.l.	0.016	0.01	0.017	0.028	0.061	0.016	<d.l.
Th	1.5	0.5	0.036	0.11	0.30	7.5	2.6	0.11	0.11	0.79
U	0.73	0.24	0.084	1.5	0.05	3.8	0.85	0.15	0.10	0.15
Eu/Eu*	1.37	1.52	4.77	3.83	2.33	1.22	1.23	2.23	2.48	2.96
Ce/Ce*	0.95	1.00	0.84	0.86	2.05	1.06	1.00	0.82	0.83	0.92
ΣREE	18.63	11.15	6.54	8.87	4.10	17.08	8.97	6.30	6.22	18.60
Y/Ho	27.65	33.04	29.12	30.04	40.02	21.90	21.48	33.09	34.91	33.38
$(LREE/HREE)_n$	0.62	0.48	1.67	1.58	1.16	0.15	0.21	0.51	0.82	0.75
Molar $(Ni/Fe) \times 10^{-4}$	0.33	0.36	–	–	0.03	0.42	0.13	0.08	–	0.25
$(Pr/Yb)_{SN}$	0.35	0.25	0.99	1.12	1.30	0.05	0.12	0.29	0.71	0.43
$(Sm/Yb)_{SN}$	0.54	0.38	1.11	1.00	0.92/	0.10	0.20	0.33	0.74	0.55

$Ce/Ce^* = 2Ce_{SN}/(La_{SN} + Pr_{SN})$ normalized to PAAS; d.l., detection limit; n.a., not analyzed.

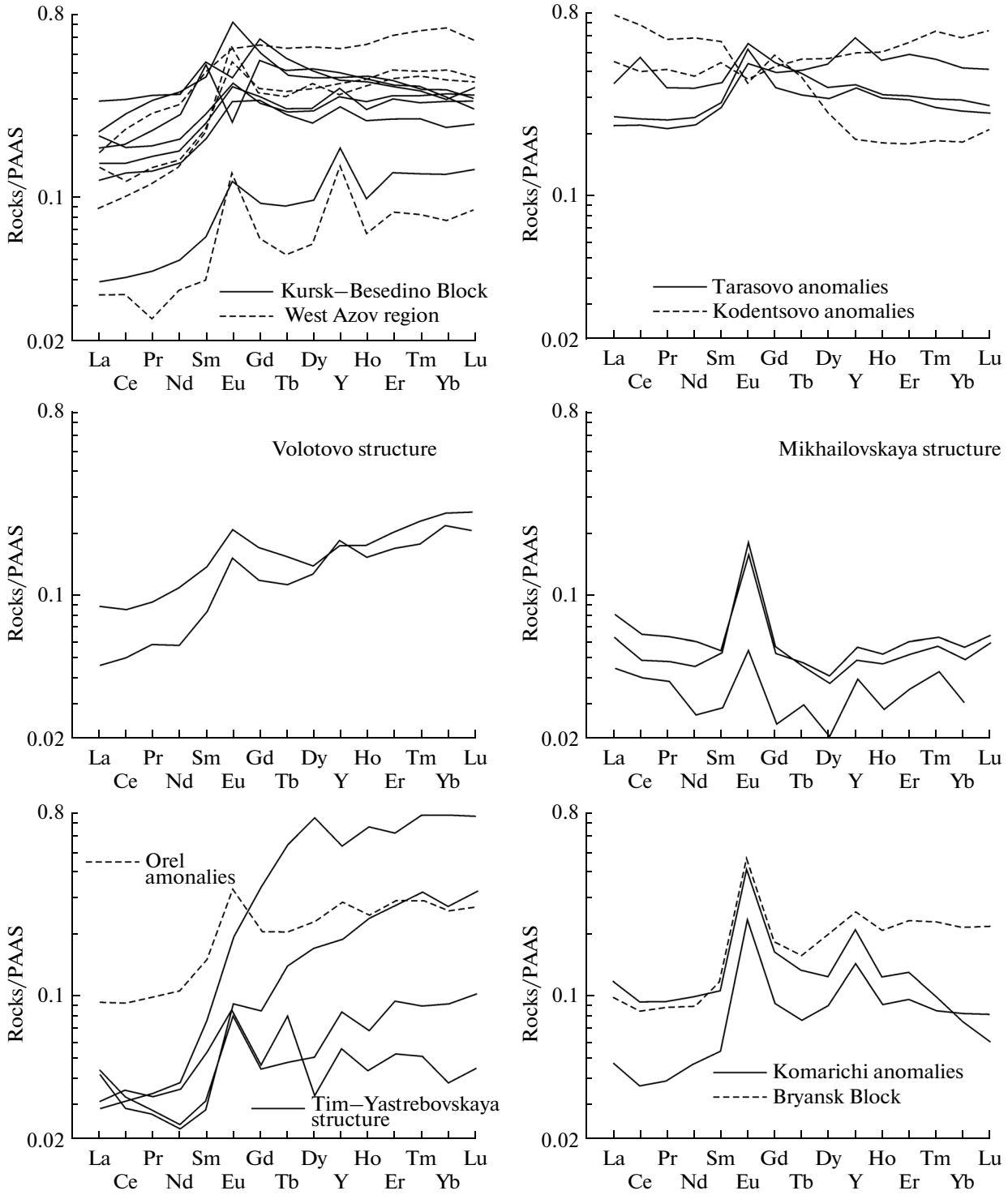

Fig. 3. REE pattern normalized to the post-Archean Australian shale (Condie, 1993) of the Precambrian BIFs of the Kursk Magnetic Anomaly and West Azov region of the Ukrainian Shield.

absence of Ce anomalies, higher values of Y/Ho (30–35) and Ni/Fe (1.45–2.75 × 10^{-4}) ratios, and higher contents of Cr (32–49 ppm, Fig. 4), Zr (17–41 ppm), and V (39–57 ppm). Let us note the high contents of Zn (149–184 ppm) and As (2.6–4.9 ppm) in comparison with Mesoarchean and Paleoproterozoic BIFs.

Another type of Neoarchean garnet–amphibole–magnetite rocks among gneisses and garnet amphibo-

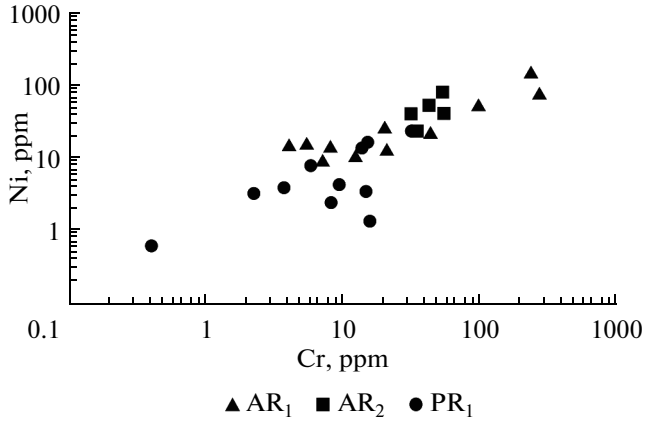

Fig. 4. Cr and Ni contents in the Precambrian BIFs of the Kursk Magnetic Anomaly and West Azov region of the Ukrainian Shield.

lites of the Kodentsovo anomalies with high content of Fe_2O_{3total} (50 wt %) and Al_2O_3 (4.2 wt %) is characterized by an elevated content of REEs (78 ppm) with dominant HREEs over LREEs, absence of positive Eu and Ce anomalies (Table 2), and low chondrite (Y/Ho) ratio of 27.

The Paleoproterozoic BIFs are distinct from Archean ones in very low contents of TiO_2 (<0.1 wt %), Al_2O_3 (<1 wt %), other major oxides, and REEs (<21 ppm). Similar REE patterns of the Paleoproterozoic BIFs from different structures and areas of the VCM (Tim–Yastrebovskaya, Volotovo, and Mikhailovskaya structures, Orel magnetic anomalies, Bryansk Block) are characterized by the absence of Ce anomalies and the presence of positive Eu and Yanomalies (Fig. 3). The $(Pr/Yb)_{SN}$ ratio, which records the enrichment in HREEs over LREEs, varies widely from 0.05 to 1.30 (0.59 on average). The values of the Y/Ho ratio also vary broadly (21–45, 32 on average). The Paleoproterozoic BIFs differ from Archean ones in the lower contents of Ni, Cr (Fig. 4), Co, and Zn and low Ni/Fe ratio (Fig. 5).

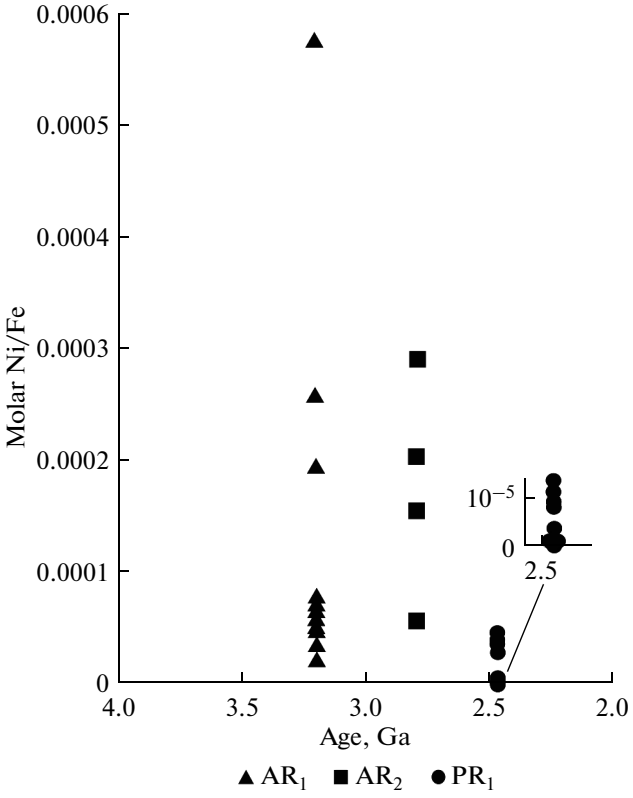

Fig. 5. Ni/Fe ratios in the Precambrian BIFs of the Kursk Magnetic Anomaly and West Azov region of the Ukrainian Shield.

INTERPRETATION OF RESULTS

The majority of chemical components of the BIFs have a hydrothermal source (Klein, 2005). Such typical geochemical features as low REE (especially LREE) contents with positive Eu anomalies are exclusively considered as evidence of hydrothermal fluid circulation in the bottom layer of marine basins (Dymek and Klein, 1988; Jacobsen and Pimentel-Klose, 1988; Klein and Beukes, 1989; Beukes and Klein, 1990; Derry and Jacobsen, 1990; Bau and Möller, 1993; Klein, 2005).

Rare Earth Elements and Yttrium

The REE contents in BIFs are always very low; however, they are distinct in the BIFs of the VCM of different age. The maximum REE contents are typical of Mesoarchean (7–60 ppm, 34 ppm on average) and especially of Neoarchean (45–79 ppm, 67 ppm on average) rocks, whereas minimum REE contents (4–21 ppm, 11.9 ppm on average) are characteristic of the Paleoproterozoic BIFs. It is noteworthy that the REE contents in Mesoarchean BIFs with and without detrital material are similar, which is evidence that insignificant clastic supply has no effect on accumulation and distribution of REEs.

Cerium in both Archean and Paleoproterozoic BIFs of the VCM is trivalent, which is reflected in the absence of Ce/Ce* anomalies and is evidence of reduced conditions in marine basins. Positive Eu/Eu* anomalies are registered in the BIFs of the VCM of all ages (Fig. 3). The character of the distribution of REEs and Y in the BIFs of the VCM is typical of marine sedimentation conditions, and a small introduction of terrigenous and volcanic material to the Mesoarchean and Neoarchean BIFs, respectively, has no influence on this. The enrichment in HREEs relative to LREEs is explained by formation of REE carbonate complexes, which leads to significantly higher sorption of LREEs (Bekker et al., 2014). In addition, LREEs are more actively absorbed on the surface of precipitating Mn and Fe hydroxides (Planavsky et al., 2010).

The fractionation of Y and Ho is also caused by the higher degree of absorption of Ho by precipitating particles of iron oxides and hydroxides (Bau et al., 1996, 1998). As in all Early Precambrian BIFs, the presence of Y anomalies and the Y/Ho ratios higher than in shales suggest the sedimentation of iron rocks under marine conditions, because yttrium is less active in reactions with precipitating particles than its geochemical analog Ho (Nozaki et al., 1997; Plavansky et al., 2010).

In comparison with shales, the Y/Ho ratio in the BIFs of the KMA of all ages varies widely from 21 to 58 (32–33 on average), suggesting the mixing of seawater (Y/Ho ~ 40–80) and a hydrothermal component (Y/Ho ~ 28). Similar Y/Ho values in Paleoproterozoic and Mesoarchean BIFs are important, because no fractionation of Y and Ho is observed in Archean BIFs and the Y/Ho ratios are close to subchondritic (Alexander et al., 2008). Probably, this occurs in volcanic sections of BIFs (Algoma type). The decreased Y/Ho values of the Neoarchean BIFs of the KMA suggest a greater hydrothermal introduction into sedimentation basins relative to the Mesoarchean and Paleoproterozoic BIFs.

Nickel

Nickel in BIFs accumulates mostly in magnetite and amphiboles (Pecoits et al., 2009; Mloszewska et al., 2012) and its contents vary periodically. The Fe-normalized Ni contents in BIFs decrease from the Paleoarchean to the Archean–Paleoproterozoic boundary (Konhauser et al., 2009), especially strongly (by a factor of two) at the boundary of 2.7 Ga. The high Ni contents in Archean BIFs are related to the eruptions of huge amounts of Ni-rich ultramafic rocks (komatiites) in the Archean, Ni from which was delivered to marine basins in a soluble state in the composition of ash or clastic material. This is clearly traced in the BIFs of the VCM. The Ni/Fe molar ratios in Mesoarchean BIFs are in a range of $0.21–0.68 \times 10^{-4}$ (0.46×10^{-4} on average) and they sharply increase ($1.9–5.7 \times 10^{-4}$) in samples with detrital material. The high values of this ratio are also detected in the Neoarchean BIFs of the Tarasovo ($1.8–2.8 \times 10^{-4}$, 2.1×10^{-4} on average) and Kodentsovo (0.54×10^{-4}) anomalies. The Ni/Fe ratios in Paleoproterozoic BIFs range from <0.01 to 0.42×10^{-4} (0.19×10^{-4} on average) (Table 3, Fig. 5).

Chromium

In studying the behavior of Cr in BIFs, it was shown (Konhauser et al., 2011) that the BIFs that formed under coastal-marine conditions or near submarine volcanic arcs and spreading zones (Algoma type) as proximal exhalative sediments are the most enriched in Cr.

The Cr distribution in the BIFs of the VCM completely corresponds to these data. The maximum Cr contents (102–228 ppm, 183 ppm on average) are typical of Mesoarchean BIFs with detrital material, and Neoarchean amphibole–magnetite rocks (Algoma type) have higher Cr contents (32–49 ppm, 43 ppm on average). Other BIF samples without clastic (volcanic) material contain less than 18 ppm Cr irrespective of age (Table 3).

Cobalt

The Co distribution is similar to that of Cr and Ni in many respects. The minerals with high Fe, Mg, Ni, and Cr contents are enriched, as a rule, in Co, especially olivine and pyroxenes from ultramafic rocks (Glassley and Piper, 1978). The continental runoff of Co was rather intense in the Archean, when the crust hosted a large amount of ultramafic rocks, and it significantly decreased in Paleoproterozoic, after the content of Co in the crust fell from 22 to 15 ppm (Condie, 1993). The high Co contents in Archean high-temperature hydrothermal fluids, which exceed by several orders of magnitude those in seawater, are probably due to the mafic and ultramafic composition of the Archean oceanic crust. For example, the Co contents in the fluids from Rainbow ultramafic-hosted hydrothermal field (Mid-Atlantic Ridge) are higher by 10^5 times than those in seawater (Douville et al., 2012). Oxygen-free conditions were favorable for migration of dissolved Co from the source (Swanner et al., 2014).

The Co distribution in the BIFs of the VCM is in agreement with these general trends. The highest Co contents are established in Mesoarchean BIFs with clastic material (Co = 12–24 ppm, 16.4 ppm on average) and Neoarchean BIFs of the Tarasovo anomalies of Algoma type (Co = 9–14 ppm, 11 ppm on average) (Table 3). Lower contents are noted in Mesoarchean BIFs free of clastic material (Co = 2.1–8.9 ppm, 4.5 ppm on average), and the lowest Co contents are typical of Paleoproterozoic BIFs (Co = 0.4–6.0 ppm, 2 ppm on average). It may be concluded that Co contents depend on the amount of detrital material in the BIFs and a hydrothermal supply of seafloor exhalations. The Co contents in pure chemogenic BIFs are very low.

Zinc

In the BIFs, the Zn/Fe values are relatively constant from the Archean to Paleozoic in spite of significantly variable geochemical characteristics of the oceans (Robbins et al., 2013). The enrichment in Zn may be related to the supply of crustal material or activity of hydrothermal systems. In seawater, zinc is present as hydroxides and carbonate complexes and its concentration depends on absorption interaction with precipitating particles of aluminosilicates, iron hydroxides, and organic complexes (Millero, 1996; Benjamin and Leckie, 1981; Zachara et al., 1988).

Zinc is a chalcophyle element and its contents are insignificant in anaerobic seawater environments, because it precipitates as sulfides. However, owing to anomalously low content of sulfate ions in the Archean and Paleoproterozoic oceans (Canfield, 1998), sulfides are not formed. Grunerite and actinolite (Mloszewska et al., 2012) and ferrous talc (Pecoits et al., 2009) are the major Zn concentrators in the BIFs.

The maximum Zn contents in the BIFs of the VCM are determined in the Neoarchean amphibole–magnetite rocks of the Tarasovo anomalies, which are closely associated with metabasalts. Its accumulation is possible both as a result of the gain of volcanic material and as a result of postvolcanic hydrothermal activity, which is consistent with the studies cited above. In contrast to Ni, Cr, and Co, the presence of detrital material in Mesoarchean BIFs has no effect on their Zn contents.

Arsenic

The clastic material and seawater have very low As contents, whereas hydrothermal fluids may be 2–500 times richer in As in the form of arsenate anions ($HAsO_4^{2-}$ and H_2AsO^{4-}; Pecoits et al., 2009). Thus, it could accumulate in sulfides and ferrous sediments. Its maximum contents are established in Neoarchean amphibole–magnetite rocks of the Tarasovo anomalies (Table 3), which implies its hydrothermal introducing related to submarine volcanism.

Uranium

Several stages of evolution of oxidation conditions of the Earth have been established as a result of recent studies of uranium cycles in BIFs (Partin et al., 2013). Stage 1 lasted from ~3.5 Ga (formation of Archean BIFs) to ~2.47 Ga (Great Oxidation Event). The BIFs of this stage have low U contents (<6.6 ppm, 0.9 ppm on average), which is explained by a limited runoff of uranium from the continents to the oceans under an anaerobic atmosphere. Thus, the oceans contained negligible contents of seawater-dissolved uranium prior to ~2.47 Ga. Its content in seawater was controlled by river runoff from the continents. The river waters contained no dissolved uranium from the weathered rocks, which are formed during oxidation. The detrital contamination was also insignificant taking into account the low U contents in the upper continental crust (2.7 ppm; Taylor and McLennan, 1985).

The significant increase in U contents in the BIFs in the period of 2.47–2.32 Ga was related to the consequences of the GOE (Partin et al., 2013). In the BIFs of the VCM irrespective of age, the U contents are very low (typically, <1 ppm), which indicates the upper age of iron deposition—no later than the GOE (~2.47 Ga).

DISCUSSION

Analyzing the distribution of major and trace (including REEs) elements in the BIFs of the VCM, we may make a conclusion on the age of formation of BIFs without an adequate stratigraphic age (Mesoarchean, Neoarchean, Paleoproterozoic), i.e., the BIFs of the Bryansk Block and the Komarichi, Tarasovo, and Kodentsovo magnetic anomalies. By geochemical indicators (low contents of REEs, Co, and Cr and low Ni/Fe ratios), the highly metamorphosed BIFs of the Bryansk Block and the Komarichi anomalies are pure chemogenic rocks typical of the Paleoproterozoic.

The BIFs of the Tarasovo anomalies exhibit higher contents of Al_2O_3, TiO_2, REEs, and trace elements and higher Ni/Fe ratios, which is typical of the Neoarchean BIFs of Algoma type. The higher Zn and As contents indicating a hydrothermal contamination and formation near the zones of volcanic activity distinguish them from the Mesoarchean BIFs.

The geochemical characteristics of BIFs of the Kodentsovo anomalies, which occur among gneisses, are undoubtedly closer to the Archean BIFs than to the Paleoproterozoic BIFs, but it is impossible to identify whether they are Mesoarchean or Neoarchean.

Thus, the Paleoproterozoic BIFs of VCM with very low contents of Al, Ti, Cr, Ni, Co, and REEs show no features of clastic or hydrothermal contamination. The low values of the Ni/Fe ratio suggest that the age of their formation is less than 2.66 Ga (Konhauser et al., 2009), which is characteristic of the boundary with a sharp drop in the level of mantle supply of Ni. On the other hand, the very low U contents (<1 ppm) point to the upper age level of iron deposition—no later than the GOE (~2.47 Ga). This is supported by the absence of Ce anomalies in Paleoproterozoic BIFs, since the BIFs older than 2.4 Ga bear no information on cerium oxidation cycles.

Several samples of Mesoarchean BIFs are characterized by higher Al_2O_3, TiO_2, Cr, and Zr contents, which indicates their low contamination by crustal material. All Neoarchean BIFs are enriched in crustal components in comparison with Mesoarchean and Paleoproterozoic BIFs, but in the case with BIFs in volcanic sequences, they could be the products of submarine volcanism and accompanying hydrothermal activity, which is evident from the higher Zn, As, and REE contents rather than the products of runoff of detrital material from the continent. The hydrothermal contamination during formation of Neoarchean and rare Mesoarchean BIFs in volcanic sequences is confirmed by higher REE, Zn, and As contents. Because the values of the Ni/Fe molar ratio in the BIFs of the Tarasovo and Kodentsovo anomalies are similar to those from Mesoarchean rocks of the Kursk–Besedino Block and West Azov region, it may be suggested that the Neoarchean rocks are older than 2660 Ma, i.e., they were formed prior to the sharp drop of the level of the mantle supply of Ni.

These conclusions are confirmed by trends of REE distribution in the BIFs of the VCM: positive Eu anomalies, absence of Ce anomalies, notable enrichment in HREEs (LREE/HREE and (Pr/Yb)SN < 1), and high Y/Ho ratios for both Archean and Paleoproterozoic rocks, which is typical of the BIFs with age of more than 2470 Ma (Bekker et al., 2014).

CONCLUSIONS

(1) The distribution of major oxides, rare earth, and trace elements in the BIFs of the Bryansk Block and Komarichi anomalies is characteristic of the Paleoproterozoic BIFs, whereas those from the Kodentsovo and Tarasovo anomalies exhibit a typical Archean distribution.

(2) Paleoproterozoic BIFs of the VCM were formed at the very beginning of the Paleoproterozoic prior to the GOE and are marine chemogenic rocks without detrital material and significant hydrothermal contamination of components.

(3) The age of Archean BIFs of the VCM is no less than 2.7 Ga. Some samples of Mesoarchean BIFs are contaminated by clastic material. The distribution of major oxides and rare earth and trace elements in BIFs of the Tarasovo anomalies is typical of BIFs of Algoma type, which were formed near the zones of volcanic activity.

Reviewers V.A. Glebovitskii and M.A. Semikhatov

REFERENCES

Alexander, A.B., Bau, M., Andersson, P., and Dulski, P., Continentally-derived solutes in shallow Archean seawater: rare earth element and Nd isotope evidence in iron formation from the 2.9 Ga Pongola Supergroup, South Africa, *Geochim. Cosmochim. Acta*, 2008, vol. 72, pp. 378–394.

Artemenko, G.V., Geochronology of the Middle Dnieper, Azov, and Kursk granite–greenstone areas, *Doctoral (Geol.-Mineral.) Dissertation*, Kiev, 1998 [in Ukrainian].

Artemenko, G.V., Shvayka, I.A., and Tatarinova, E.A., The Paleoarchean age of ultrametamorphic plagiogranites of the Kursk-Besedino block, Voronezh Crystalline Massif, *Geol. Zh.*, 2006, no. 1, pp. 84–87.

Bau, M. and Möller, P., Rare-earth element systematics of the chemically precipitated component in Early Precambrian iron formations and the evolution of the terrestrial atmosphere-hydrosphere-lithosphere system, *Geochim. Cosmochim. Acta*, 1993, vol. 57, pp. 2239–2249.

Bau, M., Koschinsky, A., Dulski, P., and Hein, J.R., Comparison of the partitioning behaviors of yttrium, rare-earth elements, and titanium between hydrogenic marine ferromanganese crusts and seawater, *Geochim. Cosmochim. Acta*, 1996, vol. 60, pp. 1709–1725.

Bau, M., Usui, A., Pracejus, B., et al., Geochemistry of low-temperature water-rock interaction: evidence from natural waters, andesite, and iron-oxyhydroxide precipitates at Nishiki-Numa Iron Spring, Hokkaido, Japan, *Chem. Geol.*, 1998, vol. 151, pp. 293–307.

Bekker, A., Holland, H.D., Wang, P.-L., et al., Dating the rise of atmospheric oxygen, *Nature*, 2004, vol. 427, pp. 117–120.

Bekker, A., Planavsky, N.J., Krapež, B., et al., Iron formations: their origins and implications for ancient seawater chemistry, in *Treatise on Geochemistry. Second ed. Vol. 9: Sediments, Diagenesis, and Sedimentary Rocks*, Amsterdam: Elsevier, 2014, pp. 561–628.

Benjamin, M.M. and Leckie, J.O., Multiple-site adsorption of Cd, Cu, Zn, and Pb on amorphous iron oxyhydroxide, *J. Colloid. Interf. Sci.*, 1981, vol. 79, pp. 209–221.

Beukes, N.J. and Klein, C., Geochemistry and sedimentology of a facies transition–from microbanded to granular iron-formation–in the early Proterozoic Transvaal Supergroup, South Africa, *Precambrian Res.*, 1990, vol. 47, pp. 99–139.

Bibikova, E.V., Bogdanova, S.V., Claesson, S., et al., Age, nature and structure of the Precambrian crust in Belarus, *Stratigr. Geol. Correl.*, 1995, vol. 3, no. 6, pp. 591–601.

Canfield, D.E., A new model for Proterozoic ocean chemistry, *Nature*, 1998, vol. 396, pp. 450–453.

Condie, K.C., Chemical composition and evolution of the upper continental crust: contrasting results from surface samples and shales, *Chem. Geol.*, 1993, vol. 104, pp. 1–37.

Derry, L.A. and Jacobsen, S.B., The chemical evolution of Precambrian seawater: evidence from REEs in banded iron formations, *Geochim. Cosmochim. Acta*, 1990, vol. 54, pp. 2965–2977.

Douville, E., Charlou, J.L., Oelkers, E.H., et al., The rainbow vent fluids (36°14′ N, MAR): the influence of ultramafic rocks and phase separation on trace metal content in Mid-Atlantic Ridge hydrothermal fluids, *Chem. Geol.*, 2002, vol. 184, pp. 37–48.

Dymek, R.F. and Klein, C., Chemistry, petrology, and origin of banded iron-formation lithologies from the 3800 Ma Isua Supracrustal Belt, West Greenland, *Precambrian Res.*, 1988, vol. 39, pp. 247–302.

Fonarev, V.I., Pilugin, S.M., Savko, K.A., and Novikova, M.A., Exsolution textures of orthopyroxene and clinopyroxene in high-grade BIF of the Voronezh Crystalline Massif: evidence of ultrahigh-temperature metamorphism, *J. Metamorphic Geol.*, 2006, vol. 24, pp. 135–151.

Glassley, W.E. and Piper, D.Z., Cobalt and scandium partitioning versus iron content for crystalline phases in ultramafic nodules, *Earth Planet Sci. Lett.*, 1978, vol. 39, pp. 173–178.

Jacobsen, S.B. and Pimentel-Klose, M.R., Nd isotopic variations in Precambrian banded iron formations, *Geophys. Rev. Lett.*, 1988, vol. 15, pp. 393–396.

Kholin, V.M., Geology, geodynamics, and metallogenic evaluation of Early Proterozoic KMA structures, *Cand. Sci. (Geol.-Mineral.) Dissertation*, Voronezh, 2001.

Kirschvink, J.L., *Late Proterozoic low-latitude global glaciation: the snowball Earth*, in *The Proterozoic Biosphere*, Schopf, J.W. and Klein, C., Eds., Cambridge: Cambridge Univ. Press, 1992, pp. 51–52.

Klein, C. and Beukes, N.J., Geochemistry and sedimentology of a facies transition from limestone to iron-formation deposition in the Early Proterozoic Transvaal Supergroup, South Africa, *Econ. Geol.*, 1989, vol. 84, pp. 1733–1774.

Klein, C., Some Precambrian banded-iron formations (BIFs) from around the world: their age, geologic setting, mineralogy, metamorphism, geochemistry, and origin, *Am. Mineral.*, 2005, vol. 90, pp. 1473–1499.

Kohnhauser, K.O., Pecoits, E., Lalonde, S.V., et al., Oceanic nickel depletion and a methanogen famine before the Great Oxidation Event, *Nature*, 2009, vol. 458, pp. 750–754.

Kohnhauser, K.O., Lalonde, S.V., Planavsky, N.J., et al., Aerobic bacterial pyrite oxidation and acid rock drainage during the Great Oxidation Event, *Nature*, 2011, vol. 478, pp. 369–373.

Kononov, N.D., Petrov, B.M., Fomenko, Yu.M., and Shevyrev, A.I., The Voronezh Crystalline Massif, in *Zhelezisto-kremnistye formatsii dokembriya Evropeiskoi chasti SSSR* (The Precambrian Banded Iron Formations in the European Part of the USSR), Kiev: Tektonika, 1988.

Millero, F.J., *Chemical Oceanography. Second Ed.*, Flordia: CRC Press, Boca Raton, 1996.

Mloszewska, A.M., Pecoits, E., Cates, N.L., et al., The composition of Earth's oldest iron formations: the Nuvvuagittuq Supracrustal Belt (Quebec, Canada), *Earth Planet. Sci. Lett.*, 2012, vols. 317–318, pp. 331–342.

Nozaki, Y., Zhang, J., and Amakawa, H., The fractionation between Y and Ho in the marine environment, *Earth Planet. Sci. Lett.*, 1997, vol. 148, pp. 329–340.

Partin, C.A., Lalonde, S.V., Planavsky, N.J., et al., Uranium in iron formations and the rise of atmospheric oxygen, *Chem. Geol.*, 2013, vol. 362, pp. 82–90.

Pecoits, E., Gingras, M.K., Barley, M.E., et al., Petrography and geochemistry of the Dales Gorge banded iron formation: paragenetic sequence, source and implications for palaeo-ocean chemistry, *Precambrian Res.*, 2009, vol. 172, pp. 163–187.

Planavsky, N.J., Bekker, A., Rouxel, O.J., et al., Rare earth element and yttrium compositions of Archean and Paleoproterozoic iron formations revisited: new perspectives on the significance and mechanisms of deposition, *Geochim. Cosmochim. Acta*, 2010, vol. 74, pp. 6387–6405.

Polyakova, T.N, Savko, K.A., and Skryabin, V.Yu., *Petrologiya metapelitov i silikatno-karbonatnykh porod Tim-Yastrebovskoi struktury (Voronezhskii kristallicheskii massiv)* (Petrology of Metapelites and Silicate-Carbonate Rocks of the Tim-Yastrebovskaya Structure, Voronezh Crystalline Massif), Voronezh: Voronezh State Univ., 2006 [in Russian].

Robbins, L.J., Lalonde, S.V., Saito, M.A., et al., Authigenic iron oxide proxies for marine zinc over geological time and implications for eukaryotic metallome evolution, *Geobiol.*, 2013, vol. 11, pp. 295–306.

Savko, K.A., Fayalite–grunerite–magnetite–quartz rocks in BIF of the Voronezh Crystalline Massif: phase equilibria and metamorphic conditions, *Petrology*, 1994, vol. 2, no. 5, pp. 540–550.

Savko, K.A. and Lebedev, I.P., Petrology of Archean phlogopite-diopside marbles of the Bryansk block of the Voronezh Crystalline Massif, *Vestn. Voronezh Univ., Ser. Geol.*, 1996, no. 2, pp. 32–42.

Savko, K.A., Petrology and tectonothermal evolution of granulites in the Bryansk block, Voronezh Crystalline Massif, *Petrology*, 1999a, vol. 7, no. 3, pp. 276–298.

Savko, K.A., Physicochemical parameters of metamorphism of eulysites from the central part of the Voronezh Crystalline Massif, *Vestn. Voronezh Univ., Ser. Geol.*, 1999b, no. 8, pp. 73–81.

Savko, K.A., Reaction textures and metamorphic evolution of spinel granulites in the Voronezh Crystalline Massif, *Petrology*, 2000, vol. 8, no. 2, pp. 165–181.

Savko, K.A. and Poskryakova, M.V., Riebeckite-aegirine-celadonite BIF at the Mikhailovskoe Iron Deposit of the Kursk Magnetic Anomaly: phase equilibria and metamorphic conditions, *Petrology*, 2003, vol. 11, no. 5, pp. 471–490.

Savko, K.A., Pilyugin, S.M., and Novikova, M.A., Mineralogy, phase equilibriums, and metamorphic conditions of Neoarchean banded iron formations within the Tarasov anomaly, *Vestn. Voronezh Univ., Ser. Geol.*, 2004, no. 2, pp. 111–126.

Savko, K.A., Phase equilibria in rocks of the Paleoproterozoic banded iron formation (BIF) of the Lebedinskoe deposit, Kursk Magnetic Anomaly, and the petrogenesis of BIF with alkali amphiboles, *Petrology*, 2006, vol. 14, no. 6, pp. 567–587.

Savko, K.A., Kotov, A.B., Sal'nikova, E.B., et al., The age of metamorphism of granulite complexes of the Voronezh Crystalline Massif: the monazite U-Pb geochronology, *Dokl. Earth Sci.*, 2010, vol. 435, no. 2, pp. 1575–1580.

Savko, K.A., Samsonov, A.V., Bazikov, N.S., and Kozlova, E.N., Paleoproterozoic granitoids of the Tim-Yastrebovskaya structure of the Voronezh Crystalline Massif: geochemistry, geochronology, and melt sources, *Vestn. Voronezh Univ., Ser. Geol.*, 2014, no. 2, pp. 56–78.

Savko, K.A., Kholina, N.V., and Larionov, A.M., The age of Neoarchean ultra-potassium rhyolites--an important geochronolical key for understanding the evolution of the Early Precambrian crust of the Voronezh crystalline massif, in *Mat. VI Ross. konf. po izotopnoi geokhronologii* (Proc. VI Russ, Conf. on Isotope Geochronology), St. Petersburg: Sprinter, 2015, pp. 247–249

Shchegolev, I.N., *Zhelezorudnye mestorozhdeniya dokembriya i metody ikh izucheniya* (Precambrian Iron Ore Deposits and Methods of their Study), Moscow: Nedra, 1985 [in Russian].

Shcherbak, N.P., Zagnitko, V.N., Artemenko, G.V., and Bartnitskii, E.N., Geochronology of great geological events in the Priazovian block of the Ukrainian Shield, in *Geokhimiya i rudoobrazovanie* (Geochemistry and Ore Genesis), Kiev, 1995, no. 21, pp. 112–128.

Shchipansky, Đ .A. and Bogdanova, S.V., The Sarmatian crustal segment: Precambrian correlation between the Voronezh Massif and the Ukrainian Shield across the Dnieper–Donets aulacogen, *Tectonophysics*, 1996, vol. 268, pp. 109–125.

Shchipanskii, A.A., Samsonov, A.V., Petrova, A.Yu., and Larionova, Yu.O., Geodynamics of the eastern margin of Sarmatia in the Paleoproterozoic, *Geotectonics*, 2007, no. 1, pp. 43–70.

Swanner, E.D., Planavsky, N.J., Lalondec, S.V., et al., Cobalt and marine redox evolution, *Earth Planet. Sci. Lett.*, 2014, vol. 390, pp. 253–263.

Taylor, S.R. and McLennan, S.M., *The Continental Crust: Its Composition and Evolution*, Oxford: Blackwell, 1985.

Zachara, J.M., Cowan, C.E., Schmidt, R.L., and Ainsworth, C.C., Chromate adsorption by kaolinite, *Clays Clay Miner.*, 1988, vol. 36, pp. 317–326.

Zhelezorudnye formatsii dokembriya KMA i ikh perspektivnaya otsenka na zheleznye rudy (Precambrian Banded Iron Formations in the Kursk Magnetic Anomaly (KMA) and their Evaluation) Golivkin, N.A., Ed., Moscow: Nedra, 1982 [in Russian].

Translated by I. Melekestseva